JCI The Journal of Clinical Investigation

Macrophage-epithelial paracrine crosstalk inhibits lung edema clearance during influenza infection

Christin Peteranderl, … , G.R. Scott Budinger, Susanne Herold

J Clin Invest. 2016;126(4):1566-1580. https://doi.org/10.1172/JCI83931.

Research Article **Infectious disease** **Pulmonology**

Influenza A viruses (IAV) can cause lung injury and acute respiratory distress syndrome (ARDS), which is characterized by accumulation of excessive fluid (edema) in the alveolar airspaces and leads to hypoxemia and death if not corrected. Clearance of excess edema fluid is driven mostly by the alveolar epithelial Na,K-ATPase and is crucial for survival of patients with ARDS. We therefore investigated whether IAV infection alters Na,K-ATPase expression and function in alveolar epithelial cells (AECs) and the ability of the lung to clear edema. IAV infection reduced Na,K-ATPase in the plasma membrane of human and murine AECs and in distal lung epithelium of infected mice. Moreover, induced Na,K-ATPase improved alveolar fluid clearance (AFC) in IAV-infected mice. We identified a paracrine cell communication network between infected and noninfected AECs and alveolar macrophages that leads to decreased alveolar epithelial Na,K-ATPase function and plasma membrane abundance and inhibition of AFC. We determined that the IAV-induced reduction of Na,K-ATPase is mediated by a host signaling pathway that involves epithelial type I IFN and an IFN-dependent elevation of macrophage TNF-related apoptosis–inducing ligand (TRAIL). Our data reveal that interruption of this cellular crosstalk improves edema resolution, which is of biologic and clinical importance to patients with IAV-induced lung injury.

Macrophage-epithelial paracrine crosstalk inhibits lung edema clearance during influenza infection

Christin Peteranderl,[1,2] Luisa Morales-Nebreda,[3] Balachandar Selvakumar,[1,2] Emilia Lecuona,[3] István Vadász,[1,2] Rory E. Morty,[1,2,4] Carole Schmoldt,[1,2] Julia Bespalowa,[1,2] Thorsten Wolff,[5] Stephan Pleschka,[6] Konstantin Mayer,[1,2] Stefan Gattenloehner,[7] Ludger Fink,[2,8] Juergen Lohmeyer,[1,2] Werner Seeger,[1,2,4] Jacob I. Sznajder,[3] Gökhan M. Mutlu,[9] G.R. Scott Budinger,[3] and Susanne Herold[1,2]

[1]Department of Internal Medicine II, University of Giessen and Marburg Lung Center (UGMLC) Giessen, Germany. [2]German Center for Lung Research (DZL). [3]Division of Pulmonary and Critical Care Medicine, Northwestern University Feinberg School of Medicine, Chicago, Illinois, USA. [4]Department of Lung Development and Remodeling, Max Planck Institute for Heart and Lung Research, Bad Nauheim, Germany. [5]Division of Influenza Viruses and Other Respiratory Viruses, Robert Koch Institut, Berlin, Germany. [6]Institute of Medical Virology and [7]Department of Pathology, Justus Liebig University Giessen, Giessen, Germany. [8]Institute of Pathology and Cytology, Wetzlar, Germany. [9]Section of Pulmonary and Critical Care Medicine, The University of Chicago, Chicago, Illinois, USA.

Influenza A viruses (IAV) can cause lung injury and acute respiratory distress syndrome (ARDS), which is characterized by accumulation of excessive fluid (edema) in the alveolar airspaces and leads to hypoxemia and death if not corrected. Clearance of excess edema fluid is driven mostly by the alveolar epithelial Na,K-ATPase and is crucial for survival of patients with ARDS. We therefore investigated whether IAV infection alters Na,K-ATPase expression and function in alveolar epithelial cells (AECs) and the ability of the lung to clear edema. IAV infection reduced Na,K-ATPase in the plasma membrane of human and murine AECs and in distal lung epithelium of infected mice. Moreover, induced Na,K-ATPase improved alveolar fluid clearance (AFC) in IAV-infected mice. We identified a paracrine cell communication network between infected and noninfected AECs and alveolar macrophages that leads to decreased alveolar epithelial Na,K-ATPase function and plasma membrane abundance and inhibition of AFC. We determined that the IAV-induced reduction of Na,K-ATPase is mediated by a host signaling pathway that involves epithelial type I IFN and an IFN-dependent elevation of macrophage TNF-related apoptosis–inducing ligand (TRAIL). Our data reveal that interruption of this cellular crosstalk improves edema resolution, which is of biologic and clinical importance to patients with IAV-induced lung injury.

Introduction

Influenza A viruses (IAV) infect cells in the alveolus and induce primary viral pneumonia, which can progress to acute respiratory distress syndrome (ARDS) with high mortality (1). IAV-induced lung injury is characterized by exaggerated inflammatory responses and loss of barrier function, resulting in edema formation and severe hypoxemia (1–4). Resolution of inflammation together with repair of the damaged epithelium and edema fluid clearance are crucial events in the recovery phase of ARDS (5). It has been demonstrated that impaired edema resolution in ARDS patients is strongly correlated with increased mortality (6, 7). Therefore, understanding the molecular mechanisms by which IAV infection decreases lung edema clearance might provide therapeutic targets to improve clinical outcome in IAV-induced ARDS.

Fluid reabsorption is driven by an osmotic gradient generated by the coordinated regulation of the apically expressed epithelial sodium channel (ENaC) and the basolaterally expressed Na,K-ATPase. Sodium ions enter the epithelial cells via ENaC and are transported out of cells by the Na,K-ATPase, which promotes the aquaporin-driven or transcellular removal of water from the alveolar airspace (8, 9). The Na,K-ATPase is a heterodimeric protein that couples the transfer of 3 sodium ions out of the cell in exchange for the intracellular transfer of 2 potassium ions with energy provided by the hydrolysis of ATP. It is therefore the major driver of vectorial sodium transport and has been shown to be an important determinant and limiting factor of net fluid clearance (10–15).

During IAV infection of the distal respiratory tract, the functional and structural impairment of the tight alveolar epithelial cell (AEC) layer, and thus the alveolo-capillary barrier results in fluid leakage from the vascular compartment into the alveolar space and persistent edema (4, 16, 17). However, the underlying mechanisms are not well understood. Recent findings suggest that an overly exuberant inflammatory response may contribute to alveolar barrier disruption via a mechanism that requires both tissue-resident and BM-derived macrophages (BMM) (4, 16, 18, 19). We have recently demonstrated that the cytokine TNF-related apoptosis–inducing ligand (TRAIL), when released in excessive amounts from aveolar macrophages (AMs) upon autocrine IFNβ stimulation, significantly contributes to IAV-induced immunopathology (4, 16).

Here, we identify a paracrine communication network between different cellular subsets within the inflamed alveolus, which we found is critical to affect alveolar fluid clearance (AFC) in IAV-induced lung injury. In vitro and in vivo IAV infection led

▶ Related Commentary: p. 1245

Conflict of interest: The authors have declared that no conflict of interest exists.
Submitted: August 4, 2015; **Accepted:** January 26, 2016.
Reference information: *J Clin Invest*. 2016;126(4):1566–1580. doi:10.1172/JCI83931.

to reduced plasma membrane expression of alveolar epithelial Na,K-ATPase and thus impaired lung edema clearance in vivo. We discovered that IAV-infected epithelial cells and macrophages, as well as noninfected neighboring epithelial cells, establish a specific communication network via epithelial type I IFN and especially the IFN-dependent, macrophage-expressed TRAIL, which determines Na,K-ATPase plasma membrane protein abundance and, thus, edema clearance during IAV infection. The identified pathways underlying this macrophage-epithelial crosstalk are amenable to therapeutic targeting to improve alveolar edema clearance in vivo and putatively improve outcome in patients with severe IAV-induced lung injury.

Results

IAV infection leads to decreased Na,K-ATPase protein abundance and impaired AFC. Murine intratracheal infection with H1N1 IAV A/PR/8/34 resulted in alveolar edema at day 7 postinfection (d7 pi) not present in PBS-treated control groups (Figure 1A, upper panel). The excessive fluid in the alveolar airspace upon IAV infection was associated with severe hypoxemia at d7 pi (Figure 1B) and substantial impairment of AFC in vivo detected at d2 and more pronounced at d7 pi (Figure 1C). We therefore assessed Na,K-ATPase α1 subunit (NKAα1) protein abundance, after in vitro H1N1 IAV infection of primary AEC. Gene expression levels of NKAα1 did not change after IAV infection (data not shown); however, the total cell protein abundance was significantly decreased at 16 hours pi (16h pi) and 24h pi in murine AEC (mAEC) as well as in in primary human AEC (hAEC) at 16h pi (Figure 1, E and F). In addition, IAV infection was associated with reduction of the immunofluorescent signal for NKAα1 in vivo, which was particularly found within highly inflamed aveolar regions but was found less within less inflamed alveolar regions; noninfected mice showed high NKAα1 expression (Figure 1A, lower panels).

Alveolar epithelial plasma membrane NKAα1 is decreased after IAV infection in vitro. Na,K-ATPase is mostly stored in intracellular compartments but contributes to active ion transport and AFC when recruited to the basolateral cell membrane (20, 21). Therefore, we assessed NKAα1 plasma membrane abundance by flow cytometry (gating strategy in Figure 1D), as well as by plasma membrane biotinylation and subsequent pulldown in in vitro–infected AEC. Both assays revealed reduced NKAα1 protein abundance at the plasma membrane in mAEC and hAEC following IAV infection (Figure 1, G–J).

Reduced alveolar epithelial plasma membrane expression of NKAα1 causes impaired AFC after IAV infection in vivo. We next investigated whether Na,K-ATPase levels were affected by IAV infection in vivo and assessed NKAα1 plasma membrane protein abundance on distal lung epithelial cells, largely comprising type II alveolar epithelial cells (Supplemental Figure 1; supplemental material available online with this article; doi:10.1172/JCI83931DS1), by flow cytometry. IAV infection resulted in a reduction of plasma membrane NKAα1 on alveolar epithelial cells in vivo already on d2 pi and most pronounced on d7 pi (Figure 2A), which correlated with the reduced fluid clearance depicted in vivo (Figure 1C). To assess if decreased levels of NKAα1 were a direct cause of reduced AFC capacities after IAV infection, we either induced overexpression of NKAα1 and NKAβ1 (22, 23) in parallel by adenoviral delivery prior to IAV infection or increased Na,K-ATPase plasma membrane abundance by treatment of AEC by the β-adrenergic agonist salbutamol (15, 24). Adenoviral overexpression of NKAα1 and NKAβ1 indeed restored total NKAα1 in IAV-infected AEC to baseline levels in vitro (Figure 2C) and also plasma membrane expressed NKAα1 in vivo (Figure 2D). Similarly, salbutamol treatment increased NKAα1 plasma membrane abundance both in vitro and in vivo (Figure 2, B and D). Importantly, increased NKAα1 expression on alveolar epithelial cells directly contributed to improved AFC after IAV infection in vivo (Figure 2E). In line, direct blockade of Na,K-ATPase activity by its specific inhibitor ouabain resulted in decreased AFC (Supplemental Figure 2).

A soluble mediator released from infected macrophages and AEC leads to decreased plasma membrane NKAα1 protein abundance. Given our previous findings that alveolar and BMM contribute to AEC damage (4, 16) and that NKAα1 was particularly reduced within strongly inflamed regions of the lung, we explored whether presence of AMs or BMM would further inhibit NKAα1 after IAV infection. Indeed, epithelial cell NKAα1 protein abundance of noninfected AEC was significantly reduced in the presence of infected AM alone and further reduced after infection of both AEC and either AM (Figure 3A) or BMM (Figure 3B). Notably, plasma membrane–expressed NKAα1 was significantly decreased on noninfected AEC in presence of IAV-infected BMM (Figure 3, C and D). As AEC and AM/BMM were cultured without direct physical contact to each other, these results suggest that paracrine crosstalk via a soluble macrophage-produced mediator leads to NKAα1 downregulation and that additional infection of AEC further reduced total and plasma membrane–expressed NKAα1 (Figure 3, C and D). We therefore investigated whether the reduction of NKAα1 at the plasma membrane after IAV infection in the AEC monoculture was similarly mediated by paracrine signaling rather than by IAV infection itself. We correlated viral protein expression (hemagglutinin, HA) to NKAα1 plasma membrane abundance (Figure 3E), and indeed, plasma membrane NKAα1 was predominantly reduced in the adjacent noninfected IAV-HA$^-$ fraction of mAEC (Figure 3F) and hAEC (Figure 3G), as well as of alveolar cells after IAV infection in vivo (Figure 3H). Furthermore, treatment of mAEC with conditioned media of infected but not of PBS-treated mAEC was sufficient to decrease NKAα1 plasma membrane protein abundance (Figure 3I).

Paracrine signaling of epithelial type I IFN– and IFN-dependent macrophage TRAIL leads to reduced plasma membrane NKAα1 protein abundance in AEC. To identify soluble factors within the AEC-macrophage crosstalk network that mediated the observed effect on NKAα1 plasma membrane expression in AECs, we analyzed coculture supernatants for proinflammatory cytokines by ELISA and cytometric bead array (data not shown). We found that IFNα — and to a minor extent IFNβ (Figure 4A and Supplemental Figure 3) — were released from infected AEC, whereas BMM did not increase IFNα release upon IAV infection (Figure 4A). We recently demonstrated that type I IFNs are potent inducers of TNF family cytokines in AM, particularly of TRAIL (4, 16). Likewise, IAV infection of BMM with IAV led to a significant release of TRAIL (Figure 4B), which was type I IFN–dependent as demonstrated by use of BMM derived from type I IFN receptor–deficient

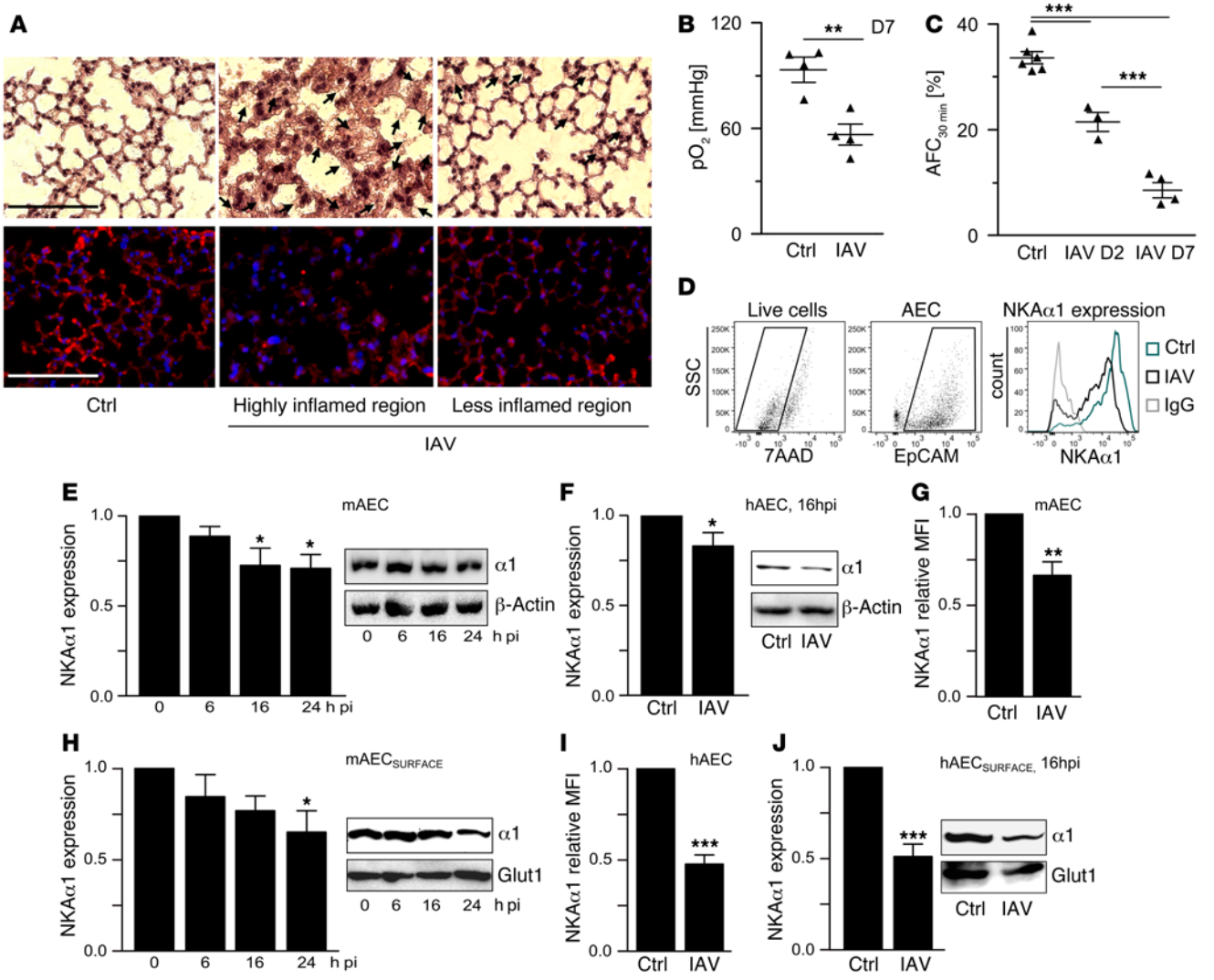

Figure 1. NKAα1 protein on the plasma membrane is decreased in a murine model of severe IAV infection. (**A**) Representative sections of $n = 3$ murine lungs d7 after PBS (ctrl) (left panel) or 500 pfu PR8 (IAV) inoculation in vivo, stained sequentially with anti-NKAα1 antibody (red) and DAPI (blue), followed by H&E staining. Sections of IAV-infected mice were taken from highly inflammatory (middle panel) and less inflammatory regions (right panel). Scale bars: 50 μm; arrows mark edematous regions. (**B** and **C**) Arterial partial pressure of oxygen (pO_2) (**B**) and in vivo AFC measurements (**C**) d7 pi after inoculation of PBS or PR8. (**D**) Gating strategy showing representative dot plots for live cells ($7AAD^-$), epithelial cells ($EpCAM^+$), and representative histograms of $NKA\alpha1^+$ staining or the respective IgG control from murine AEC cultures. SSC, side scatter. (**E** and **F**) Densitometric quantification of immunoblots of NKAα1 in relation to β-actin at the indicated time points in total cell lysates of mAEC (**E**) or hAEC (**F**) inoculated in vitro with PBS or PR8 for 24 hours. (**G** and **I**) Relative MFI of NKAα1 detected by FACS on live mAEC (**G**) or hAEC (**I**) treated in vitro with PBS (ctrl) or PR8 (IAV) at MOI 0.1 for 24 or 16 hours, respectively. (**H** and **J**) Densitometric analysis of NKAα1 expression in comparison to the housekeeping protein glucose transporter 1 (Glut1) within the cell surface fraction of PR8-infected mAEC at the indicated time points (**H**) or hAEC 16h pi (**I**). Values of PBS-treated control conditions were normalized to 1. Representative blots and bar graphs or dot plots show means ±SEM of 7–9 independent experiments for **B**, **C**, **E**, **F**, and **H** and 5–6 independent experiments for **G**, **I**, and **J**. Statistical significance was analyzed by unpaired Student's *t* test (**B**, **F**, **G**, **I**, and **J**) or by 1-way ANOVA and post-hoc Tukey (**C**, **E**, and **H**). $^*P < 0.05$; $^{**}P < 0.01$; $^{***}P < 0.005$.

(*Ifnar*$^{-/-}$) mice (Figure 4C). AEC did not release TRAIL in response to IAV infection (Figure 4B). Treatment of uninfected AEC with either recombinant IFNα (rIFNα) or rTRAIL decreased NKAα1 protein abundance at the plasma membrane, and combined treatment with both IFNα and TRAIL reduced NKAα1 to similar levels as coinfection of AEC and BMM (Figure 4D). rIFNβ at levels found when released by infected AEC did not affect NKAα1 levels (Supplemental Figure 3). When using *Ifnar*$^{-/-}$ AEC to block paracrine IFNα signaling between A/PR/8/34 (H1N1)–infected (PR8-infected) and noninfected AEC in monoculture, NKAα1 abundance was rescued to baseline levels at 24h pi, whereas *Trail*$^{-/-}$ AEC still displayed a strong decrease in NKAα1 protein abundance (Figure 4E). Moreover, transfer of conditioned media from either PBS-treated or PR8-infected AEC to *Ifnar*$^{-/-}$ AEC did not reduce NKAα1 plasma membrane abundance (Figure 4F), suggesting that in absence of macrophages, NKAα1 surface downregulation was solely dependent on signaling through type I IFN. We next performed coculture infections using AEC and BMM from WT, *Ifnar*$^{-/-}$, *Trail*$^{-/-}$, or *Dr5*$^{-/-}$ (TRAIL receptor) mice and assessed NKAα1 plasma membrane abundance after IAV infection. These

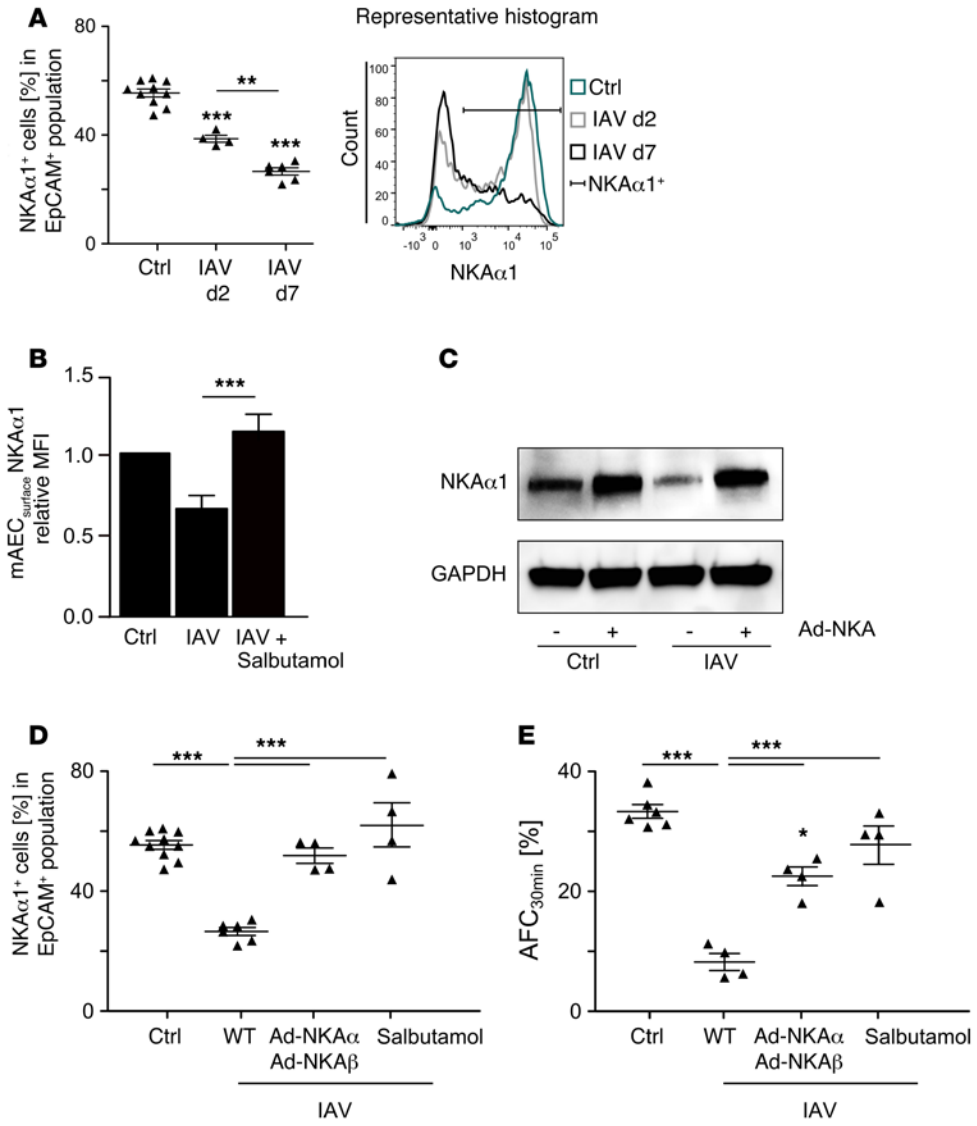

Figure 2. Reduced alveolar epithelial plasma membrane expression of NKAα1 causes impaired AFC after IAV infection in vivo. (**A**) Flow cytometric analysis of NKAα1 subunit expression on EpCAM+ epithelial cells from distal lung homogenate. WT mice were inoculated with PBS (ctrl) or PR8 (IAV) and sacrificed d2 or d7 pi. (**B**) Relative MFI of NKAα1 detected by FACS on live mAEC inoculated with PBS (ctrl) or PR8 at MOI 0.1 (IAV) and treated with 50 μM salbutamol. (**C**) Representative Western blot of 3 independent experiments blotting mAEC cell lysates for NKAα1 or GAPDH 72 hours after transfection with adenoviruses carrying NKAα1 or NKAβ1 at MOI 5 and 24 hours after PR8 infection at MOI 0.1. (**D** and **E**) WT mice were inoculated with PBS (ctrl) or PR8 (IAV) at d3 after intratracheal infection with adenoviruses overexpressing NKAα1 (Ad-NKAα) and NKAβ1 (Ad-NKAβ) or treated with 10 mg/kg salbutamol i.p. at d3 and d5. Mice were sacrificed at d7 after IAV infection. (**D**) Flow cytometric analysis of NKAα1 subunit expression on EpCAM+ epithelial cells from distal lung homogenate. (**E**) In vivo measurements of AFC rates over a time interval of 30 minutes. Graphs show single data points plus means ±SEM of 4–10 independent experiments for **A**, **D**, and **E**. Data sets depicting control conditions are identical to Figure 1C (AFC) and Figure 3A (NKAα1 expression) and included for better comparison between experimental conditions. Bar graph (**B**) represents means ±SEM of 3 independent experiments. Nonbracketed asterisk indicate statistical significance to control conditions. Statistical significance was analyzed by 1-way ANOVA and post-hoc Tukey. $^{**}P < 0.01$; $^{***}P < 0.005$.

studies revealed that lack of IFNAR signaling in AEC, together with lack of TRAIL in BMM, fully prevented NKAα1 downregulation in AEC. Partial blockade of the IFN-TRAIL signaling loop by combination of *Ifnar*$^{-/-}$ AEC with WT BMM (allowing BMM TRAIL action), or of either WT AEC with *Trail*$^{-/-}$ BMM or *Dr5*$^{-/-}$ AEC with WT BMM (allowing AEC type I IFN signaling), correspondingly resulted in partial decrease of plasma membrane NKAα1 (Figure 4G). Addition of recombinant human IFNα and/or recombinant human TRAIL to cultured hAEC reduced their ability for vectorial water transport as measured by changes in FITC-dextran concentrations in the apical versus basal medium of confluent hAEC to a similar extent as IAV infection (Figure 4H), whereas vectorial water transport of hAEC cocultured with primary human AM was significantly increased in the presence of neutralizing antibodies directed against IFNα and TRAIL after IAV infection (Figure 4I). Together, these data indicate that IAV-induced downregulation of NKAα1 and reduced ability for fluid transport depend on a signaling network between AEC and macrophages, involving epithelial type I IFN– and IFN-dependent macrophage TRAIL.

The TRAIL-mediated reduction of NKAα1 levels is induced independently of epithelial cell apoptosis. Previous work on the role of macrophage-released TRAIL during IAV infection demonstrated its contribution to extrinsic AEC apoptosis induction and to loss of barrier function (4, 16). To exclude that the observed effects of TRAIL on NKAα1 expression levels in noninfected AEC were caused by TRAIL-mediated induction of apoptosis, we inhibited activation of the effector caspase-3 by addition of the specific inhibitor Z-DEVD (25, 26) after IAV infection. In vitro and in vivo treatment with Z-DEVD resulted in significantly reduced levels of apoptotic alveolar epithelial cells after IAV infection for 24 hours and 7 days, respectively (Supplemental Figure 4, A and C). Moreover, application of Z-DEVD at d5 and d6 pi in vivo resulted in reduced activation of caspase-3 in AEC at d7 pi (Supplemental Figure 4D). However, NKAα1 plasma membrane expression was not significantly altered after IAV infection by inhibition of caspase-3 activation, both in vitro as well as in vivo (Supplemental Figure 4, B and E). Accordingly, AFC rates were reduced to similar levels at d7 pi in IAV-infected mice or IAV-infected mice

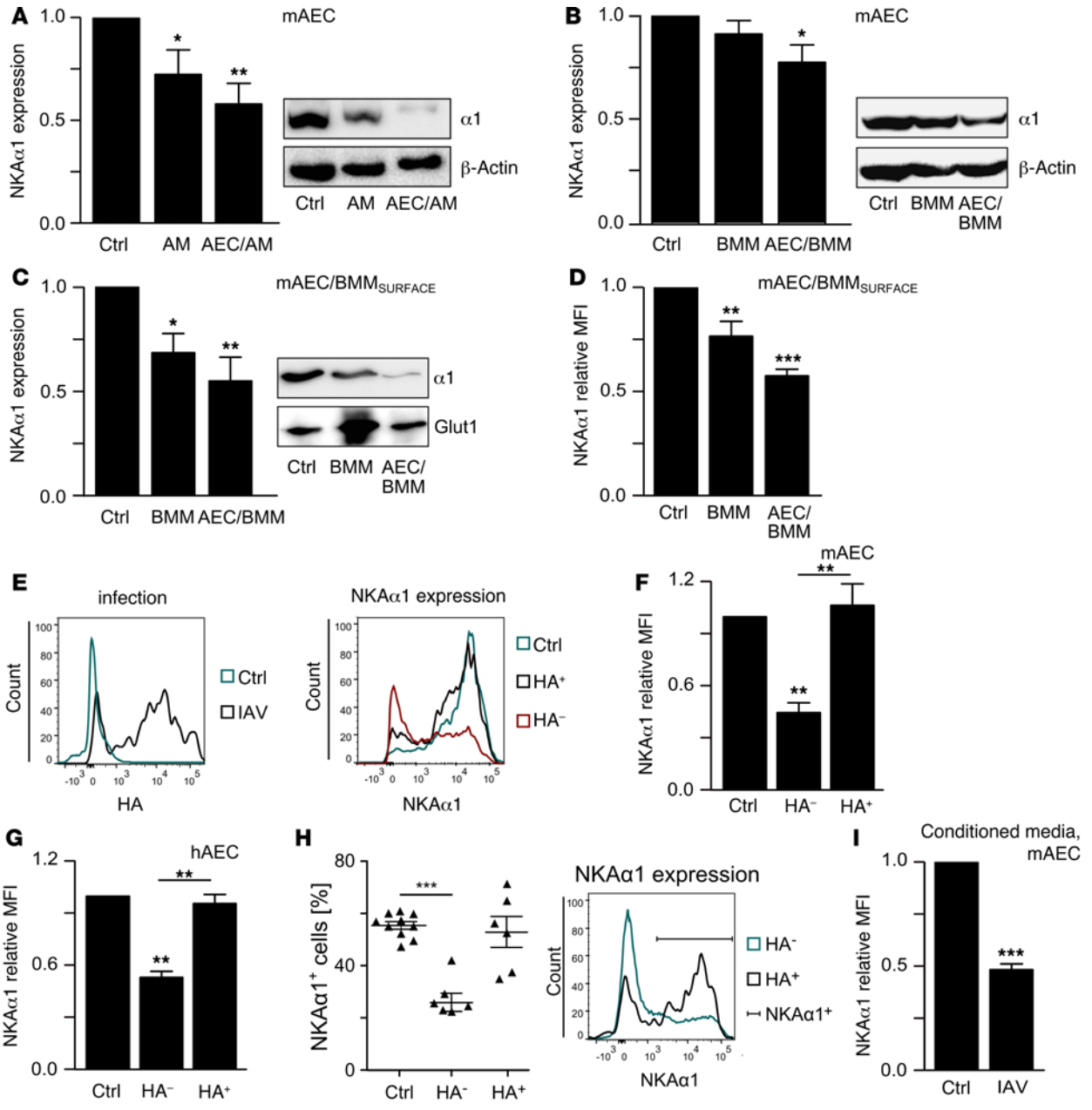

Figure 3. Epithelial plasma membrane–expressed Na,K-ATPase is decreased by a soluble mediator released from infected macrophages and AEC. (**A** and **B**) Densitometric quantification of Western blot of NKAα1 expression compared with β-actin at 24h pi in total cell lysates of mAEC after coculture with AM (**A**) or BMM (**B**) without infection (ctrl), infection of only macrophages (AM; BMM), or of both cell types (AEC/AM; AEC/BMM). (**C**) Densitometric analysis of NKAα1 expression compared with glucose transporter 1 (Glut1) within the cell surface fraction of 24h pi in PR8-infected mAEC cocultured with BMM. (**D**) Relative MFI of NKAα1 detected by FACS on live mAEC cocultured with BMM. (**E**) Gating strategy showing representative histograms for viral HA expression and NKAα1 expression on PBS-treated ctrl, IAV-infected HA$^+$, or HA$^-$ AEC. **F** and **G** depict NKAα1 MFI of HA$^+$ vs. HA$^-$ cell populations in mAEC (**F**) or hAEC (**G**) 24h pi with PR8 in comparison with PBS-treated cells (ctrl). (**H**) Flow cytometric analysis of NKAα1 subunit expression on EpCAM$^+$ epithelial cells from distal lung homogenate. NKAα1 subunit expression was analyzed in AEC of PBS-treated mice (ctrl) or on the HA$^+$ vs. HA$^-$ cell population of AEC isolated from PR8-inoculated WT mice sacrificed at d7 pi. (**I**) Analysis of NKAα1 MFI of mAEC treated for 2 hours with conditioned media from 16 hours infected (IAV) or PBS-treated (ctrl) cells. For **A**–**D**, **F**, **G**, and **I**, values of PBS-treated control conditions were normalized to 1. Representative blots, histograms, and bar graphs showing means ±SEM of n = 8–10 experiments (**A**–**C**), n = 6 (**D** and **F**), n = 3 (**G**), n = 6–10 (**H**), and n = 4 (**I**). Data depicting control conditions in **H** are identical to2**A** and are included for better comparison between experimental conditions. Statistical significance was analyzed by 1-way ANOVA and post-hoc Tukey. *P < 0.05; **P < 0.01; ***P < 0.005.

treated with Z-DEVD (Supplemental Figure 4F). Together, these data demonstrate that TRAIL-induced reduction of plasma membrane–expressed NKAα1, and its effects on net AFC are mediated independently of the induction of alveolar epithelial apoptosis.

The IFN/TRAIL-dependent reduction of NKAα1 plasma membrane abundance is mediated via AMPK. Given that Na,K-ATPase endocytosis was reported to be mediated by activation of AMP-activated protein kinase (AMPK) during lung injury–associated

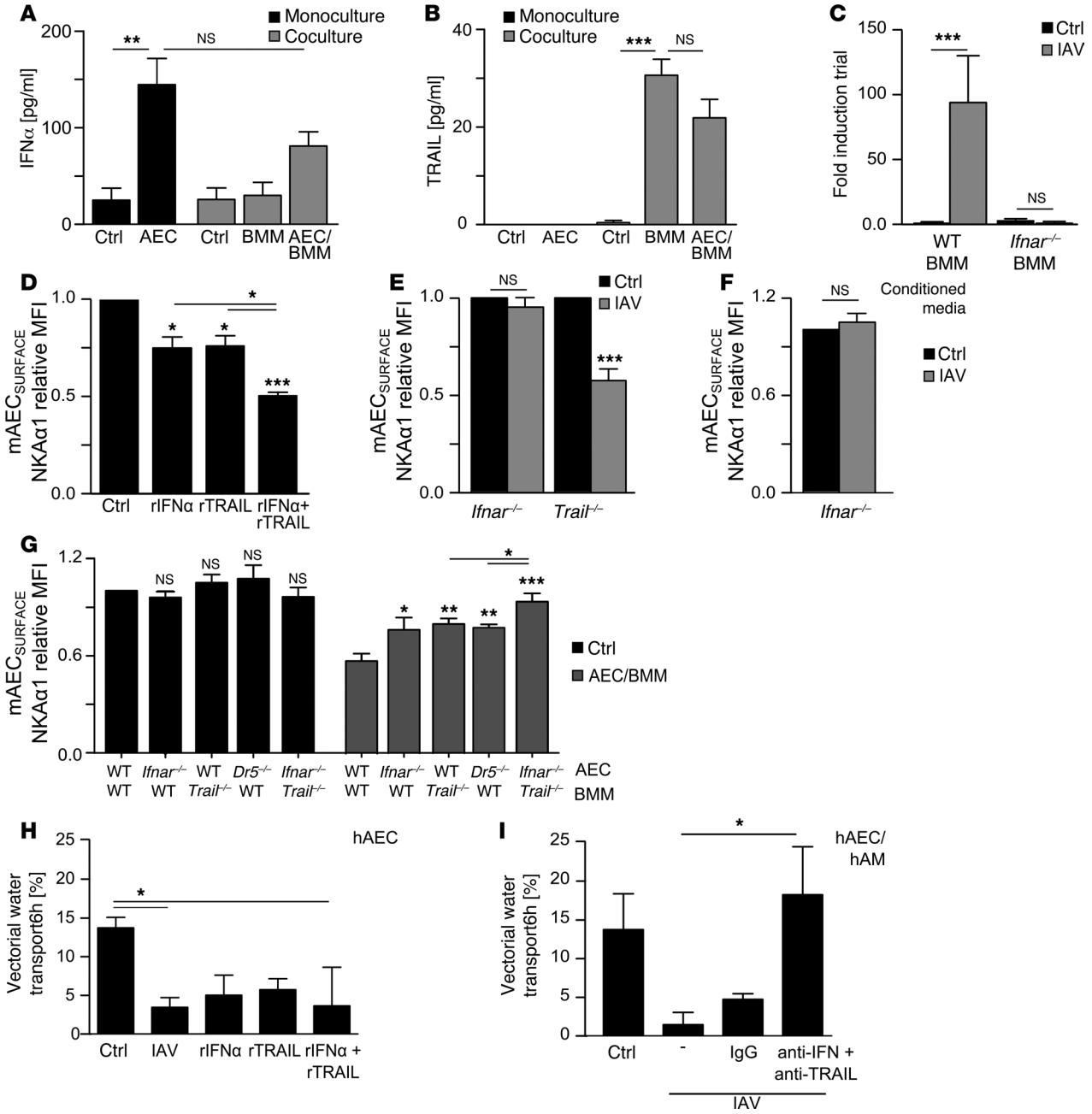

Figure 4. PR8-induced loss of Na,K-ATPase surface expression is dependent on an IFN-TRAIL signaling loop involving epithelial IFNα and type I IFN–induced macrophage TRAIL. (**A** and **B**) IFNα (**A**) and TRAIL (**B**) concentrations of AEC mono- and coculture supernatant 24h pi quantified by ELISA. mAEC were monocultured and inoculated in vitro with PBS (ctrl) or PR8 (AEC) or cocultured with BMM without infection (ctrl), with infection of only macrophages (BMM), or with infection of both cell types (AEC/BMM). (**C**) TRAIL mRNA expression quantified by qPCR in BMM isolated from WT or *Ifnar*$^{-/-}$ mice noninfected (ctrl) or PR8-infected (IAV) at 16h pi. (**D**–**G**) NKAα1 relative MFI on/of mAEC treated with 25U/ml mouse rIFNα or/and 100 pg/ml mouse rTRAIL for 16 hours (**D**); mAEC derived from *Ifnar*$^{-/-}$ or *Trail*$^{-/-}$ mice inoculated with PBS (ctrl) or PR8 (IAV) 24h pi (**E**); mAEC derived from *Ifnar*$^{-/-}$ mice inoculated for 2 hours with conditioned media from PBS (ctrl) or PR8 (IAV) WT AEC infected for 16 hours (**F**); and mAEC derived from WT, *Ifnar*$^{-/-}$, or *Dr5*$^{-/-}$ mice cocultured with BMM from WT or *Trail*$^{-/-}$ mice and infection of none (ctrl) or both cell types (AEC/BMM) in vitro (**G**). Value of control conditions were normalized to 1. (**H** and **I**) Vectorial water transport of hAEC monoculture 6 hours after inoculation with PBS (ctrl), PR8 (IAV), rIFNα (150 pg/ml), and/or rTRAIL (100 pg/ml) or in coculture with human AM without additional treatment (–), in presence of neutralizing antibodies against human IFNα (0.5 μg/ml) and human TRAIL (0.1 μg/ml) (anti-IFN + anti-TRAIL) or the respective IgG controls (IgG). hAEC maintained barrier integrity in all assay conditions (Supplemental Figure 9). Bar graphs represent means ±SEM of 4–6 independent experiments (**A**, **B**, and **E**–**I**), 3 independent experiments (**C**), and 6–8 independent experiments (**D**). Statistical significance was analyzed by Student's *t* test (**F**) or 1-way ANOVA and post-hoc Tukey (**A**–**E** and **G**–**I**). $*P < 0.05$; $**P < 0.01$; $***P < 0.005$.

epithelial dysfunction (27, 28), we investigated if AMPK was involved in regulation of NKAα1 abundance in response to IAV-induced paracrine signaling events. AMPK was indeed activated after IAV infection in AEC monocultures and AEC/BMM cocultures (Figure 5, A and B), as demonstrated by phosphorylation of the AMPK downstream substrate acetyl-CoA carboxylase (pACC) (29). Incubation of AEC with conditioned media of IAV-infected AEC and treatment with rTRAIL or rIFNα were sufficient to induce AMPK activation (Figure 5, C and D). Treatment of AEC with the AMPK activator AICA-Riboside (AICAR) (30, 31) led to decreased plasma membrane NKAα1 in noninfected AEC and, importantly, chemical inhibition of AMPK by Compound C (32) restored NKAα1 levels in infected AEC and in cocultured AEC in presence of infected BMM (Figure 5, E and F). In addition, adenoviral overexpression of a dominant-negative AMPK (DN-AMPK) in human lung epithelial cells (A549, ATCC) rescued NKAα1 expression after IAV infection (Supplemental Figure 5A). We found that chemical inhibition of the AMPK upstream calcium/calmodulin-dependent protein kinase kinase β (CaMKKβ) (33) by STO-609 in mAEC or siRNA knockdown of CaMKKβ in A549 resulted in complete inhibition of AMPK activation and restored surface NKAα1 abundance in IAV infection (Figure 5, G and H, and Supplemental Figure 5B). In addition, chelation of intracellular calcium needed for CaMKKβ activation by BAPTA-AM increased NKAα1 abundance on mAEC after IAV infection (Figure 5G). Inhibition of another possible upstream kinase of AMPK, the TGFβ activated kinase 1 (TAK1), by (5Z)-7-Oxozeanol (34) caused partial inhibition of AMPK activity without affecting NKAα1 expression (Figure 5, G and H). Accordingly, inhibition of Na,K-ATPase function by ouabain or IAV infection decreased, whereas inhibition of AMPK or CaMKKβ prevented the reduction in fluid transport after IAV infection (Figure 5I), demonstrating that IFN/TRAIL-induced loss of membrane NKAα1 involved a CaMKKβ/AMPK-dependent pathway.

Consistent with the results from our in vitro infection model, inhibition of the intracellular kinase AMPK by intratracheal instillation and overexpression of adenoviral-expressed DN-AMPK in AEC prior to infection in vivo (Supplemental Figure 6A) prevented the IAV-induced reduction in NKAα1 plasma membrane abundance and in AFC in vivo at d2 pi (Figure 6, A and B). Additionally, pharmacological inhibition of AMPK signaling in vivo by application of Compound C at d5 pi significantly increased NKAα1 plasma membrane abundance and AFC at d7 after IAV infection (Figure 6, C and D). Neither DN-AMPK instillation nor Compound C treatment impacted on viral clearance (Supplemental Figure 6B and data not shown).

IFN and BMM-released TRAIL contribute to reduced NKAα1 plasma membrane abundance and impaired AFC in vivo and are amenable to therapeutic targeting after IAV infection. We next investigated whether Na,K-ATPase levels were also dependent on the IFN/TRAIL signaling network in vivo. Interestingly, *Ifnar*$^{-/-}$ mice (deficient for both IFNα ligation by the alveolar epithelium and for IFNβ-dependent production of TRAIL by macrophages) were protected from IAV-induced reduction of NKAα1 plasma membrane expression at d7 pi (Figure 7A). Consistent with our in vitro findings demonstrating that TRAIL released from BMM mediated the reduction of membrane NKAα1 abundance during IAV infection, both *Trail*$^{-/-}$ mice and mice deficient for C-C chemokine receptor type 2 (*Ccr2*$^{-/-}$), which are unable to recruit macrophages from the BM to the lung after IAV-infection (35), were protected from NKAα1 loss on distal lung epithelial cells in response to IAV infection when compared with WT animals (Figure 7, A and B). Moreover, we demonstrate, by intrapulmonary transfer of BMM flow-sorted (Supplemental Figure 7) from the lungs of WT or *Trail*$^{-/-}$ mice at d7 after IAV infection into infected *Ccr2*$^{-/-}$ mice, that rescue of NKAα1 expression in *Ccr2*$^{-/-}$ mice at d7 pi is lost in the presence of WT BMM but maintained after transfer of *Trail*$^{-/-}$ BMM (Figure 7B). Accordingly, the IFN/TRAIL-mediated loss of surface NKAα1 significantly reduced AFC in WT mice after IAV infection but not in *Ifnar*$^{-/-}$, *Trail*$^{-/-}$, or *Ccr2*$^{-/-}$ mice (Figure 7C), which corresonded with decreased edema accumulation as quantified by wet-to-dry lung weight ratios in *Ifnar*$^{-/-}$ and *Trail*$^{-/-}$ mice (Supplemental Figure 8). Additionally, fluid clearance was completely restored in *Ccr2*$^{-/-}$ mice that were supplemented with *Trail*$^{-/-}$ BMM but not in *Ccr2*$^{-/-}$ mice receiving WT BMM (Figure 7D). Moreover, in vivo targeting of the IFN/TRAIL signaling network by administration of anti-IFNα and anti-TRAIL neutralizing antibodies resulted in enhanced NKAα1 protein abundance on the alveolar epithelium and significantly improved AFC capacities in IAV-infected WT mice, resulting in decreased edema formation and reduced morbidity, as demonstrated by body weight loss, and reduced overall morbidity scoring (Figure 8, A–D, and Supplemental Table 1). These data highlight a crucial role for the paracrine crosstalk involving IFN and macrophage-released TRAIL signaling for impairment of Na,K-ATPase–driven alveolar edema clearance capacity after IAV infection in vivo and suggest that targeting this axis is a promising approach to improve fluid clearance in humans after IAV-induced ARDS.

Discussion

Influenza virus pneumonia is characterized by infection of airway and alveolar epithelial cells and can rapidly progress to ARDS with dismal clinical outcome (1, 3). A functional impairment of the alveolar epithelial barrier after IAV infection results in pulmonary edema accumulation and impaired fluid reabsorption, which is closely correlated to mortality in ARDS patients (6, 7). Here, we report a mechanism by which a paracrine communication network between different populations of infected and adjacent cells in the alveolus downregulates alveolar epithelial Na,K-ATPase and thus inhibits AFC in response to IAV infection.

Our data demonstrate that the plasma membrane NKAα1 protein abundance is reduced after IAV infection, indicating that the key function of Na,K-ATPase — active sodium transport out of the cell — is impaired (11, 12). Vectorial sodium and fluid clearance is a coordinated process that requires the electrochemical gradient generated by the basolateral Na,K-ATPase, thereby constituting the driving force of edema reabsorption. Sodium and water transport can also be regulated by the apically located ENaC and by chloride channels such as the cystic fibrosis transmembrane receptor (CFTR). In previous work, investigators reported that the levels of ENaC and CFTR were reduced in response to viral infection via a direct interaction with the viral matrix protein (36, 37). In contrast, we found that plasma membrane Na,K-ATPase protein abundance was disproportionately

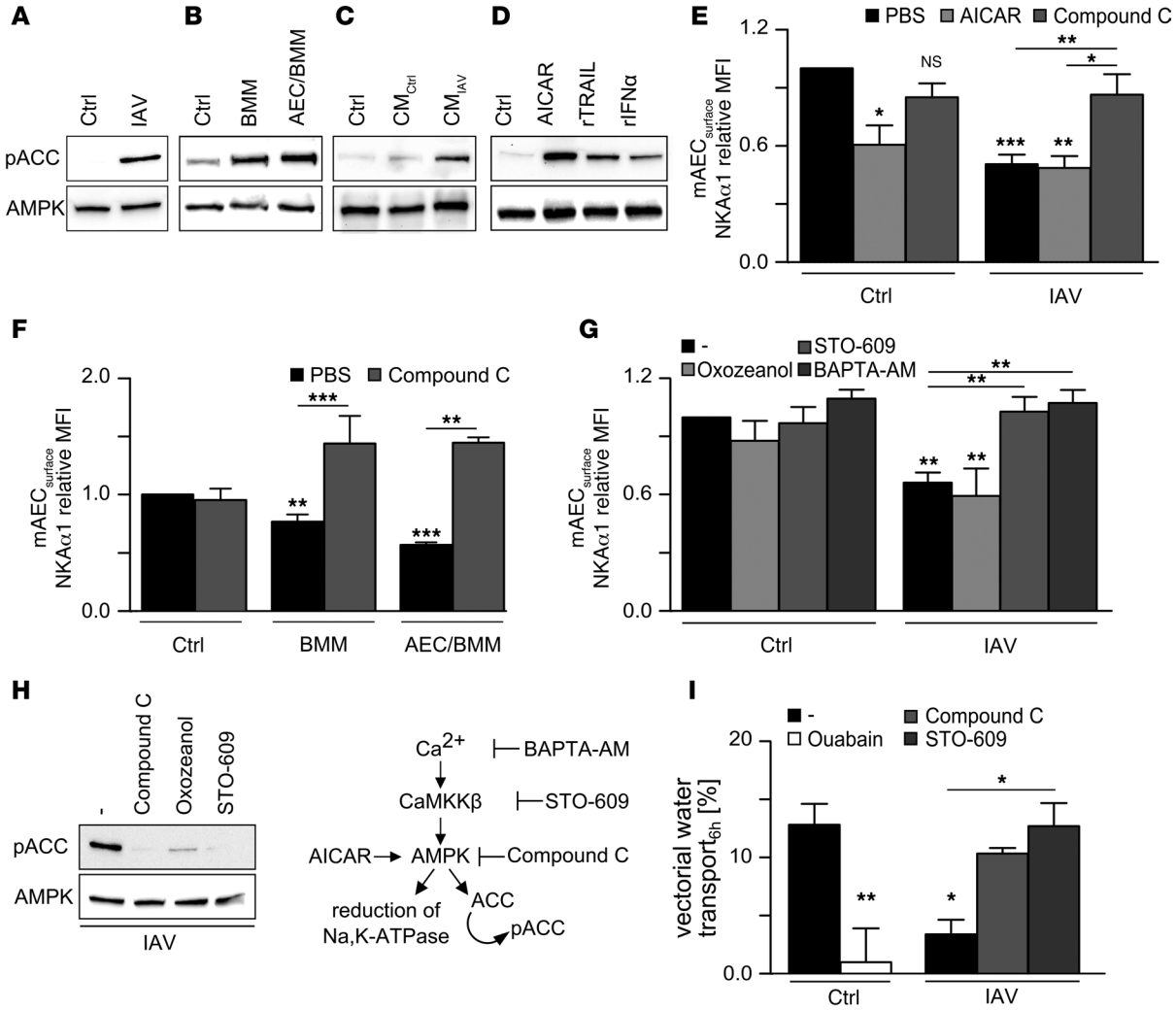

Figure 5. IAV-induced loss of NKAα1 surface expression is mediated by activation of AMPK. (**A**–**D**) Representative Western blots of n = 3–4 independent experiments of AMPK (62 kDa) and the AMPK substrate pACC (280 kDa) mAEC treated with PBS (ctrl) or PR8 (IAV) (**A**) for 24 hours. (**B**) Cocultures of murine AEC and BMM were left uninfected (ctrl); only macrophages were infected (BMM) or both cell types were infected (AEC/BMM). (**C**) mAEC were treated with conditioned media (CM) of 16 hours PR8-infected (IAV) or PBS-treated (ctrl) mAEC for 2 hours. (**D**) mAEC treated with the AICAR (1 mM), rTRAIL (100 g/ml) , or rIFNα (25 U/ml) for 16 hours. (**E**–**G**) Relative MFI of NKAα1 on mAEC inoculated with PBS (ctrl) or PR8 (IAV) for 24 hours without additional treatment or in presence of 1 mM AICAR or 20 μM Compound C (**E**); on mAEC cocultured with BMM without infection (ctrl), with infection of only macrophages (BMM), or with infection of both cell types (AEC/BMM) without additional treatment or in presence of 20 μM Compound C (**F**); on mAEC inoculated with PBS (ctrl) or PR8 (IAV) and incubated for 24 hours without additional treatment or in presence 0,1 μM TAK1 inhibitor (5Z)-7-Oxozeanol or the 0,5 μM CaMKKβ inhibitor STO-609 or 10 μM of the Ca^{2+} chelator BAPTA-AM (**G**). (**H**) Representative Western blot of n = 3–4 independent experiments of AMPK and pACC from 24 hours PR8-infected mAEC without additional treatment or in the presence of 20 μM Compound C, 0,1 μM (5Z)-7-Oxozeanol, or the 0,5 μM STO-609 and schematic depiction of the used inhibitors. (**I**) Vectorial water transport of confluent hAEC culture 6 hours after inoculation with PBS (ctrl) or PR8 (IAV) without additional treatment (–), in the presence of 25 μM Ouabain, 10 μM Compound C, or 0.5 μM STO-609. Bar graphs represent means ±SEM of 4–6 independent experiments. Values of PBS-treated control conditions were normalized to 1. Statistical significance was analyzed by 1-way ANOVA and post-hoc Tukey. *P < 0.05; **P < 0.01; ***P < 0.005.

reduced in neighboring, noninfected epithelial cells, suggesting that NKAα1 reduction is not mediated by direct interaction with a viral component but relies on paracrine signals released from the infected epithelial cells and macrophages. These findings highlight the need to understand influenza A infection in the context of integrated signaling networks involving different cell populations in the lung. Using a coculture system, we demonstrate the importance of epithelial IFNα- and IFN-induced macrophage TRAIL, which downregulated the AEC NKAα1 both in the presence and absence of IAV infection.

The type I IFNs play a complex role in the immune response to IAV infection. They are rapidly produced by AECs after viral infection to activate antiviral transcriptional programs in both epithelial and immune cells in the lung that are important for viral clearance. Furthermore, they may play a role in limiting the severity of the immune response via the production of IL-10 (38–40). Accordingly, IFNs have been suggested as potential therapeutic strategies to promote anti-IAV host defenses, particularly when applied as prophylactic treatment or early after onset of the infection (41, 42). Our data, however, indicate that

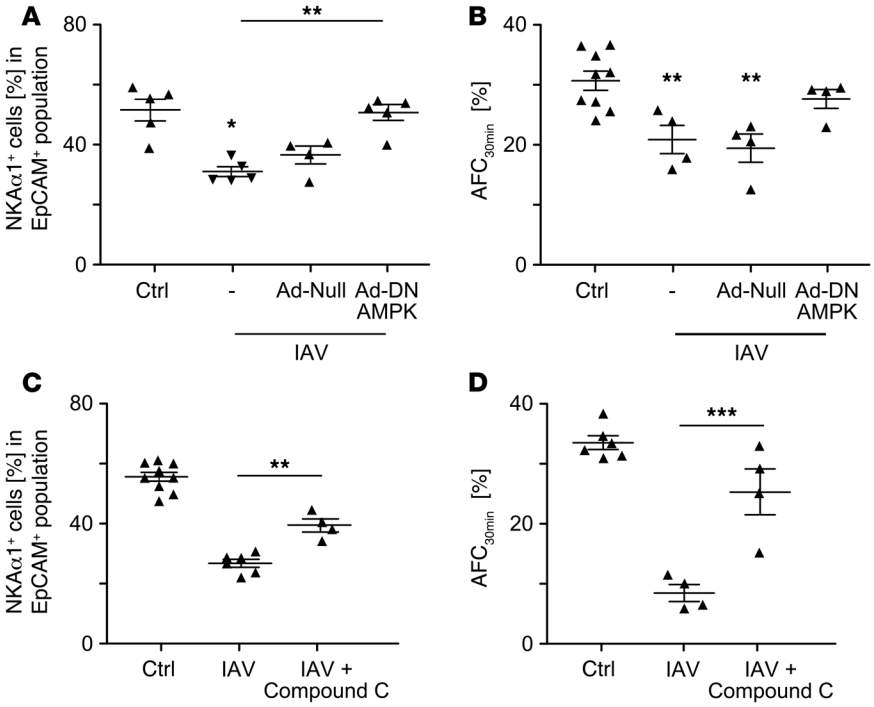

Figure 6. IAV-induced loss of NKAα1 surface expression is mediated by AMPK in vivo. (**A** and **B**) WT mice were inoculated with PBS (ctrl), Ad-Null, or Ad–DN AMPK for d7 prior to infection with PBS or IAV (Udorn) at d2 pi. (**A**) Flow cytometric analysis of NKAα1 subunit expression on AEC. (**B**) In vivo measurements of AFC rates over a time interval of 30 minutes. (**C** and **D**) WT mice were inoculated with PBS (ctrl) or PR8 (IAV) and treated with 20 mg/kg Compound C i.p. at d5 pi. Mice were sacrificed at d7 pi. (**C**) Flow cytometric analysis of NKAα1 subunit expression on AEC. (**D**) In vivo measurements of AFC rates over a time interval of 30 minutes. Graphs show means ±SEM of n = 4–5 (**A**), 4–9 (**B**), 4–9 (**C**), and 4–6 (**D**) independent experiments. Data set depicting control conditions in **C** and **D** are identical to Figure 1C (AFC) and Figure 3A (NKAα1 expression) and were included for better comparison between experimental conditions. Nonbracketed asterisk indicate statistical significance to control conditions. Statistical significance was analyzed by 1-way ANOVA and post-hoc Tukey. $^{**}P < 0.01$; $^{***}P < 0.005$.

at later time points, when the infection has spread to the alveolar compartment and progresses to lung injury, IFNs may also have a detrimental effect, evidenced by imbalanced inflammation and loss of crucial AEC functions such as edema clearance.

An important source of IFN and other proinflammatory cytokines in IAV-induced innate immune responses are AM- and CCR2-recruited BMM (43–45). Tissue resident AM play key roles in sensing viral infection and activating the initial innate and later adaptive immune responses to IAV infection (46). In concert with the macrophage populations recruited upon infection, they establish a proinflammatory environment by production and release of mediators such as IFN, leading to enhanced viral clearance and better disease outcomes (43, 47). However, it is well recognized that excessive production of cytokines during IAV infection contributes to lung injury, which impacts severity and outcome (48, 49), as shown for highly pathogenic avian influenza H5N1 or the pandemic 2009 H1N1 virus (50, 51). In particular, resident and recruited macrophages have been attributed as key roles in amplifying lung injury after IAV-infection by orchestrating an overly exuberant inflammatory response to IAV infection, worsening IAV-induced lung inflammation, lung injury severity, and mortality and hampering resolution of inflammation (4, 16, 44–48, 49, 50). In this regard, we and others revealed that IFNβ-induced autocrine activation of the death ligand TRAIL in BMM substantially deteriorates lung injury by promoting AEC injury after IAV infection (16, 52). Our current data provide important insights into these mechanisms, revealing a role of AEC-produced IFNα and macrophage-produced IFNβ-dependent TRAIL signaling within the alveolar cell-cell communication network in promoting impairment of epithelial barrier function and alveolar fluid homeostasis.

TRAIL has been widely associated with induction of extrinsic apoptosis in a variety of cells, including leukocyte subsets and cancer cells, via DR5 (53, 54). In the current study, we provide evidence that the macrophage TRAIL/epithelial DR5 interaction exerts a role in virus-induced lung injury by activating the energy sensor AMPK. Of note, we demonstrated that TRAIL/AMPK-mediated reduction of NKAα1 plasma membrane abundance and impairment of AFC was independent of TRAIL-induced epithelial cell apoptosis induction in vivo (4, 16), as inhibition of AEC apoptosis by application of Z-DEVD did not impact on NKAα1 reduction after IAV infection. Activation of the metabolic sensor/regulator AMPK, under normal conditions, upregulates ATP generating and downregulates ATP-consuming mechanisms to promote cellular survival during metabolic stress (34, 55, 56). Of note, Herrero-Martín et al. demonstrated that rTRAIL was able to activate AMPK in immortalized epithelial cells and, thus, promote autophagy, a cytoprotective mechanism rendering cells more resistant to deleterious challenges (57), highlighting the complexity of the IFN/TRAIL network in cellular injury and protection in response to cellular stress.

The Na,K-ATPase has been well documented to be targeted for downregulation via a pathway that requires AMPK and subsequent activation of PKCζ in response to stimuli that threaten metabolic homeostasis, including alveolar hypercapnia and hypoxia (27, 28). We demonstrate activation of AMPK signaling by paracrine mediators in response to IAV infection, resulting in reduced vectorial sodium transport. Inhibiting AMPK in vivo by DN-AMPK or Compound C treatment attenuated the Na,K-ATPase downregulation and restored AFC rates in IAV-infected mice. These data highlight AMPK as a critical regulator of AFC in pulmonary injury in vivo, suggesting it as a therapeutic target for the treatment of IAV (58). At low levels, however, IFN/TRAIL- and AMPK-mediated reductions in vectorial sodium transport and fluid clearance in the IAV-infected lung may be beneficial, particularly during early stages of the disease when viral replication occurs and viral loads still increase. It has been reported that alterations of sodium currents within the IAV-infected cell show

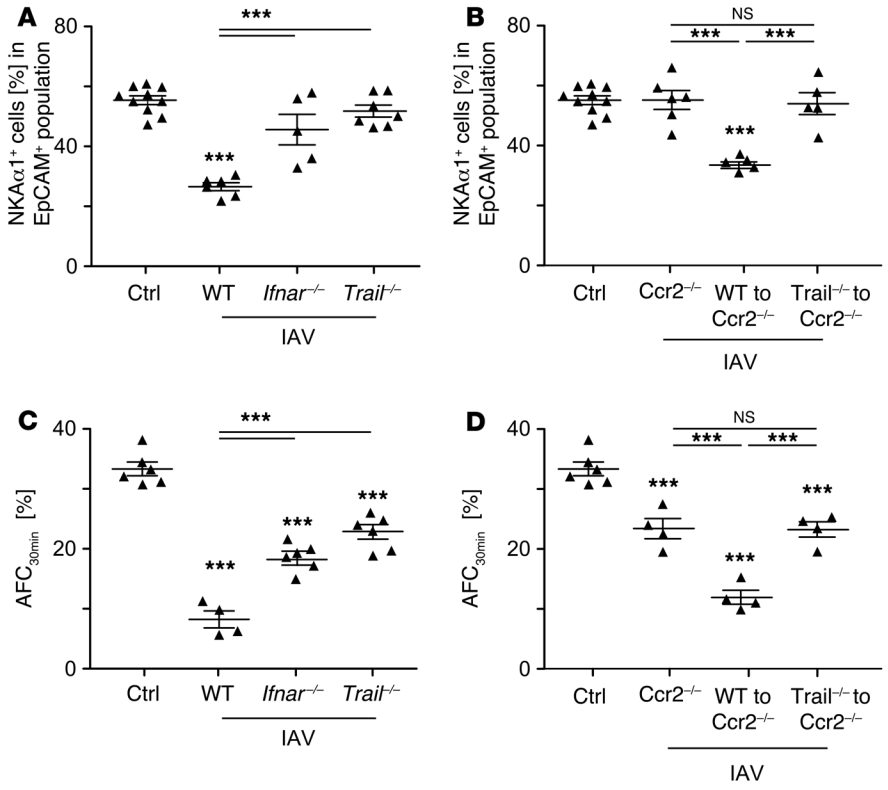

Figure 7. IAV-induced reduction of epithelial NKAα1 surface expression and AFC capacity require the presence of IFNAR and macrophage-released TRAIL in vivo. (**A** and **B**) Flow cytometric analysis of NKAα1 subunit expression on EpCAM+ epithelial cells from distal lung homogenate. (**C** and **D**) In vivo measurements of AFC rates over a time interval of 30 minutes. (**A** and **C**) WT, *Ifnar*$^{-/-}$, or *Trail*$^{-/-}$ mice were inoculated with PBS (ctrl) or PR8 (IAV) and sacrificed d7 pi. (**B** and **D**) *Ccr2*$^{-/-}$ mice were inoculated with PR8 (IAV) and sacrificed d7 pi without further intervention (*Ccr2*$^{-/-}$) or after intratracheal transfer of flow-sorted alveolar BMM from d7 infected WT (WT to *Ccr2*$^{-/-}$) or *Trail*$^{-/-}$ (*Trail*$^{-/-}$ to *Ccr2*$^{-/-}$) mice at d3 pi. Viral loads were not significantly altered between experimental groups (data not shown). Graphs show single data points plus means ±SEM of 5–10 independent experiments for **A** and **B** and 4–6 independent experiments for **C** and **D**. Data sets depicting control conditions are similar to Figure 1C (AFC) and Figure 3A (NKAα1 expression). Nonbracketed asterisk indicate statistical significance to control conditions. Statistical significance was analyzed by unpaired Student's *t* test (**B**) or by 1-way ANOVA and post-hoc Tukey. ***$P < 0.005$.

an adverse effect on viral replication (59). Therefore, the resulting changes in intracellular sodium or potassium might interfere with viral signaling, providing an antiviral defense strategy for the infected cell. Alternatively, reduced Na,K-ATPase function might represent activation of a stress response pathway, perhaps secondary to changes in intracellular calcium, that reduces the susceptibility of neighboring epithelial cells to viral infection (59). Consistent with this hypothesis, we found that signaling through IFNAR and DR5 by IFN and TRAIL, respectively, activates AMPK via a pathway that requires CaMKKβ, which is in turn activated by increases in intracellular calcium (58). While the links between calcium signaling and the AMPK during influenza A infection have not been completely elucidated, previous studies have shown that, in hypoxic conditions, an influx of extracellular calcium through stromal interaction molecule 1–activated (STIM1-activated) calcium release–activated calcium channels (CRAC channels) can lead to CaMKKβ- and AMPK-mediated endocytosis of Na,K-ATPase (27). Wang et al. demonstrated that the calcium-dependent tyrosine kinase Pyk2 interacts with the IFNAR-associated tyrosine kinases Jak1/Tyk2 (60), providing a possible link to CaMKKβ activation.

Our in vitro studies provide complementary lines of evidence demonstrating an additive role for epithelial-produced IFNα- and IFN-dependent macrophage TRAIL in the downregulation of Na,K-ATPase plasma membrane protein abundance during IAV infection. Concordant with our in vitro findings, *Ifnar*$^{-/-}$ mice deficient in the IFNα/β receptor, and thus compromised in both epithelial IFN crosstalk and IFN-dependent induction of macrophage TRAIL expression, displayed less reduction of Na,K-ATPase and were less impaired in AFC after IAV challenge. *Trail*$^{-/-}$ mice and mice lacking BMM recruitment from the circulation (*Ccr2*$^{-/-}$) were similarly protected from IAV-induced epithelial Na,K-ATPase downregulation. Of course, we cannot fully exclude that additional factors (e.g., infection-induced activation of intracellular pathways) affecting Na,K-ATPase function rather than mere surface expression (e.g., ion or ATP affinity or channel open probability) might have further influence on net AFC in our different in vivo models, as we observe substantially but not fully restored AFC rates ranging between similar levels in all gene-deficient mice applied (*Ifnar*$^{-/-}$, *Trail*$^{-/-}$, and *Ccr2*$^{-/-}$).

Further investigation on the effect of TRAIL released from recruited BMM after infection was performed via pulmonary transfer of WT but not *Trail*$^{-/-}$ BMM into *Ccr2*$^{-/-}$ mice after IAV infection, which led to decreased NKAα1 abundance and AFC similar to the decrease observed in IAV-infected WT mice and demonstrated the crucial role for TRAIL-expressing macrophages in the inhibition of AFC in vivo. We acknowledge that, in these studies, we did not address effects on overall survival, nor the consequences of TRAIL-deficiency on virus clearance, but we could importantly show that therapeutic blockade of the IFN/TRAIL network by neutralizing antibodies in vivo proved to increase NKAα1 expression and AFC after IAV infection. Considering that anti-TRAIL treatment was recently demonstrated to elicit profound effects in attenuating IAV-induced barrier disruption and to prevent pneumococcal superinfection (61), we suggest that therapeutic targeting of the here described signaling axis will not only ameliorate AFC after IAV infection, but will furthermore protect from TRAIL-mediated lung injury and complications thereof. We anticipate that targeting particularly macrophage TRAIL alone or together with epithelial

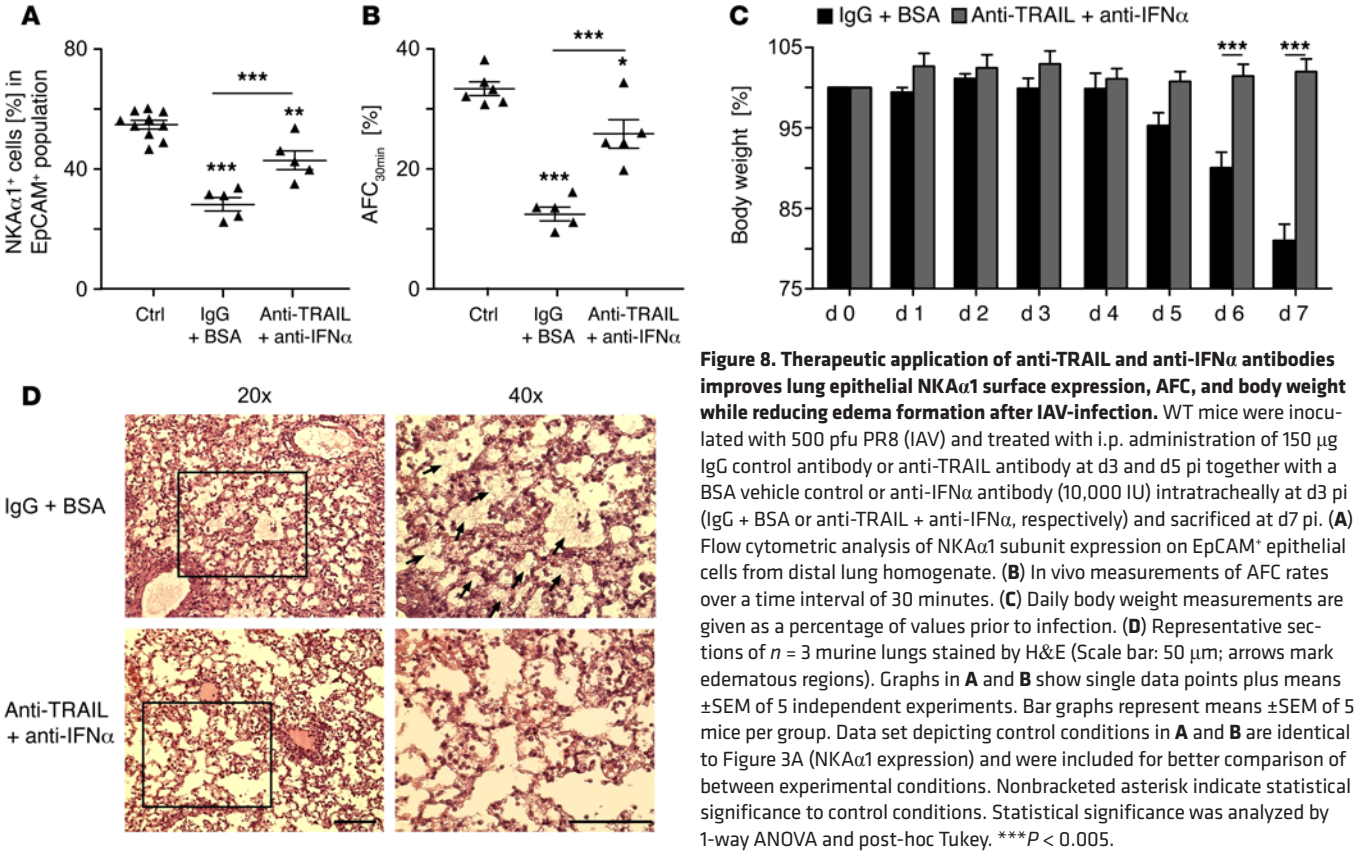

Figure 8. Therapeutic application of anti-TRAIL and anti-IFNα antibodies improves lung epithelial NKAα1 surface expression, AFC, and body weight while reducing edema formation after IAV-infection. WT mice were inoculated with 500 pfu PR8 (IAV) and treated with i.p. administration of 150 μg IgG control antibody or anti-TRAIL antibody at d3 and d5 pi together with a BSA vehicle control or anti-IFNα antibody (10,000 IU) intratracheally at d3 pi (IgG + BSA or anti-TRAIL + anti-IFNα, respectively) and sacrificed at d7 pi. (**A**) Flow cytometric analysis of NKAα1 subunit expression on EpCAM+ epithelial cells from distal lung homogenate. (**B**) In vivo measurements of AFC rates over a time interval of 30 minutes. (**C**) Daily body weight measurements are given as a percentage of values prior to infection. (**D**) Representative sections of $n = 3$ murine lungs stained by H&E (Scale bar: 50 μm; arrows mark edematous regions). Graphs in **A** and **B** show single data points plus means ±SEM of 5 independent experiments. Bar graphs represent means ±SEM of 5 mice per group. Data set depicting control conditions in **A** and **B** are identical to Figure 3A (NKAα1 expression) and were included for better comparison of between experimental conditions. Nonbracketed asterisk indicate statistical significance to control conditions. Statistical significance was analyzed by 1-way ANOVA and post-hoc Tukey. ***$P < 0.005$.

AMPK downstream signaling might be beneficial with respect to alveolar barrier protection and edema reabsorption, without compromising antiviral host defense.

In conclusion, we describe a paracrine pathway in the IAV-infected lung that links macrophage and epithelial signaling to the downregulation of the Na,K-ATPase in the noninfected fraction of AECs. This decrease is mediated by AEC-released IFNα directly and is strongly amplified through IFNα/β-induced release of TRAIL from recruited macrophages, resulting in inhibition of lung edema clearance (Figure 9). A timely modulation of this pathway might represent a novel strategy to improve fluid reabsorption and, thus, outcomes in IAV-induced lung injury and ARDS.

Methods

Supplemental Methods are available online with this article.

Mice. WT C57BL/6 mice were purchased from Charles River Laboratories. *Trail*$^{-/-}$ mice (62) were provided by AMGen. U. Kalinke (Paul-Ehrlich Institute, Erlangen, Germany) provided *Ifnar*$^{-/-}$ mice (63). *Dr5*$^{-/-}$ mice were a gift from T. Mak (Campbell Family Institute for Breast Cancer Research, University of Toronto, Toronto, Ontario, Canada) (64). *Ccr2*$^{-/-}$ mice were obtained from W. Kuziel (University of North Carolina Medical School, Cahpel Hill, North Carolina, USA; ref. 65). All transgenic lines were backcrossed to the C57BL/6 background. Mice were housed under pathogen-free conditions.

Cell isolation and culture. Primary mAEC or hAEC were isolated as previously described (16, 66), seeded on 4 μm–pore size transwells (Corning Inc.), and cultured for 3 and 5 days, respectively, prior to experiments. AEC suspensions with a purity >90% were used for further experiments. Murine resident AMs were isolated by bronchoalveolar lavage as described (16) and cultured for 2 hours before treatment. Human resident AMs were gained from bronchoalveolar lavage fluid (BALF) of patients who did not show any accumulation of recruited inflammatory cells according to differential counts of pappenheim-stained cytospins. BMM were isolated from femurs and tibias and cultured in the presence of mouse recombinant granulocyte/macrophage-CSF (GM-CSF) at 25 ng/ml for 10 days.

Infection protocols. Cells were infected with PR8 at a multiplicity of infection (MOI) of 0.1 as previously described (16). For coculture experiments, bottom-seeded AM or BMM were combined with AEC seeded on transwells after infection of only macrophages or of both cell types with PR8. Of note, an abortive replication cycle occurred in AM and BMM, as described in Högner et al. (16), and ensured that in the AM/BMM infection–only conditions, no virus was transferred to the epithelial cell layer excluding AEC infection. For in vitro experiments, recombinant murine TRAIL (R&D Systems, 100 pg/ml), recombinant murine GM-CSF (R&D Systems, 25 ng/ml) recombinant mouse IFNα and -β (PBL Interferon Source, 25 U/ml; R&D Systems, 10–100 ng/ml), recombinant human IFNα (R&D Systems, 150 pg/ml), recombinant human TRAIL (R&D Systems, 100 pg/ml), anti–human IFNα neutralizing antibody (R&D Systems, 0.5 μg/ml), anti–human TRAIL neutralizing antibody (R&D Systems, 0.1 μg/ml), and the following chemical inhibitors were used: AICAR, AMPK inhibitor Compound C, (5Z)-7-Oxozeanol (Curvularia sp), STO-609 (all Calbiochem) and BAPTA-AM (Invitrogen). Conditioned media of 16h-infected mAEC cultured in 6-well plates was transferred to uninfected mAEC

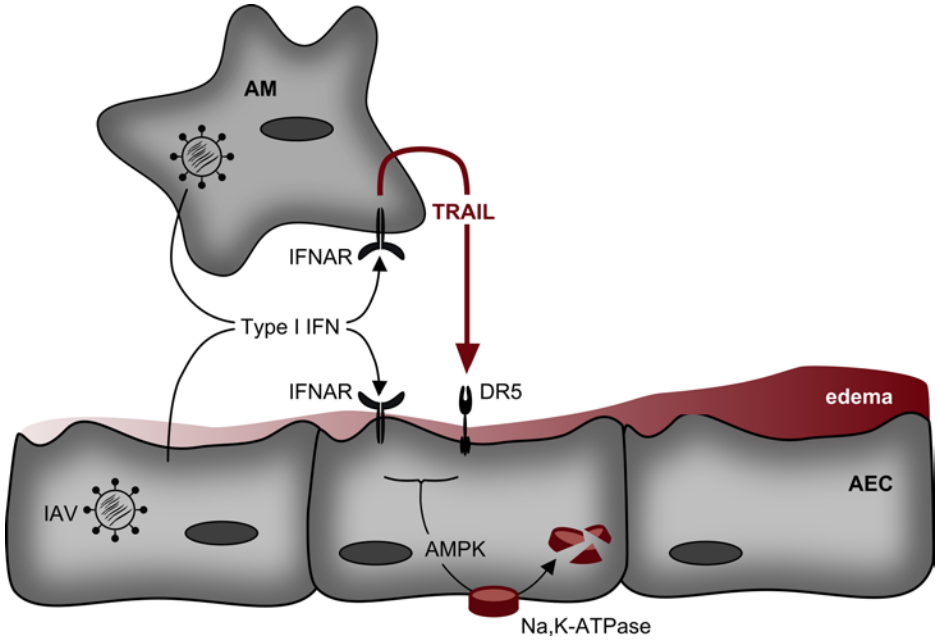

Figure 9. Model of type I IFN–mediated loss of Na,K-ATPase–mediated edema clearance in IAV infection. IAV infection results in AEC release of IFNα and induction of IFNβ-dependent release of TRAIL in AMs. Ligation to their receptors, IFNAR and particularly DR5, results in activation of the stress kinase AMPK. Activation of AMPK initiates degradation and reduction of Na,K-ATPase abundance on the cell plasma membrane and impacts on fluid reabsorption, leading to the persistence of lung edema after IAV infection.

cultured in 12-well plates and incubated for 2 hours. For in vivo infection, mice were intratracheally inoculated with 500 plaque-forming units (pfu) PR8 or 10^5 pfu A/Udorn/307/1972 (H3N2, also known as Udorn) diluted in 70-μl sterile PBS. Endotracheal delivery of adenovirus was performed at 1×10^9 pfu in 50% surfactant vehicle as described previously (24). Adenoviruses carrying either no additional construct (Ad-Null) — or expressing DN-AMPK, Ad-NKAα1, or Ad-NKAβ1 — were cloned at ViraQuest Inc. Of note, NKAβ1 — which was shown to be a crucial mediator for correct heterodimerization of the Na,K-ATPase (22, 67) — was coexpressed to ensure presence of sufficient levels of NKAβ1 to support functional Na,K-ATPase formation.

Of note, transduction efficiency was >90% in AEC, as verified by FACS for mCherry in $EpCAM^+$ cells (not shown). Neutralizing antibodies against IFNα (10,000 IU/mouse, rabbit polyclonal Ab to mouse IFNα, PBL Interferon Source) were administered intratracheally at d3 pi, and neutralizing antibodies against TRAIL (150 μg/mouse, LEAF anti-mouse CD253, BioLegend) were given i.p. at d3 and d5 pi as established previously (16). Infected mice were monitored 1–3 times per day.

In vivo measurement of AFC. The rate of fluid removal from the alveolar airspace was measured by assessment of changes in Evans blue–tagged albumin in an iso-osmolar alveolar instillate over 30 minutes as previously described (24). In short, mice were anesthetized, placed on a heating pad, and maintained in supine position. Body temperature was monitored using an anal probe and maintained at 37°C with heating pad and lamp. After reaching stable anesthesia, mice were cannulated with a shortened 18-gauge i.v. catheter, paralyzed with 2.0 mg/kg pancuronium bromide applied i.p., and ventilated via catheter connected to a mouse respirator (Harvard Apparatus) using a tidal volume of 10 ml/kg (equivalent of 0.2 ml) at a frequency of 160 breaths per minute and 100% of oxygen, as described by Hardiman et al. (68). Iso-osmolar NaCl solution (324 mOsm; 300 μl) containing 5% Evans blue–tagged (0.15 mg/ml) bovine serum albumin were installed via the catheter over a time period of 30 seconds, followed by 0.1 ml of air; then, mice were ventilated over 30 minutes. Evans blue concentrations, directly correlating with the amount of BSA in the solution, were analyzed from the initial instillate and the reaspirated fluid using a microplate reader (Bio-Rad, 620-nm filter) and AFC was calculated as follows: $AFC = 1 - (C_0/C_{30})$, where C_0 is the protein concentration before instillation and C_{30} is the protein concentration of the sample reaspirated after 30 minutes of ventilation.

Ex vivo measurement of vectorial water transport. Primary human AEC were seeded in 0.4 μm–pore size transwell cell culture dishes (Corning Inc.) and cultured until achieving electrochemical resistances of ≥800 Ω/cm^2 as measured by Millicell-ERS2 device (EMD Millipore). Cells were infected with PR8 at MOI 0.1 or PBS treated for 1 hour at 37°C and then supplied with 3 mg/ml 70 kDa FITC-dextran–labeled (Sigma-Aldrich) cell culture media including selected inhibitors at indicated concentrations. After 6 hours of incubation at 37°C, apical and basal media were analyzed for FITC-dextran concentration (FL_x 800, Bio-Tek). Cells were analyzed microscopically for bound FITC-dextran without apparent differences in the treatment groups. Vectorial water transport was calculated by changes in FITC-dextran concentration between apical (C_a) and basal (C_b) media in comparison with starting conditions (C_0): $[1 - (C_0/C_a)] - [1 - (C/C_b)]$.

Histology. Lungs were clipped at the trachea, perfused with 4% paraformaldehyde (PFA), removed, and fixed for 24 hours in 4% PFA. Lungs were embedded in Paraffin (Leica ASP200S), cut into 5-μm thick sections, and either stained with NKAα1 (clone C464.6, EMD Millipore) after antigen retrieval with 10 mM sodium citrate at 95°C for 20 minutes or stained with H&E (Merck). Analysis was performed with an EVOS FL imaging system (Thermo Fisher Scientific).

Cell surface labeling and Western blot. Cell surface labeling and Western blot were performed as previously described (16, 69). For immunostaining, the following antibodies were used: NKAα1, AMPKα (clone 40H9) and phospho-ACC (clone S79, both Cell Signaling Technology), polyclonal Glut1 (catalog 07-1401, EMD Millipore), β-actin (clone Poly6221, BioLegend), GAPDH (clone 14C10, Cell Signaling Technology), secondary mouse or rabbit HRP (clones 7076 and 7074, Cell Signaling Technology). Bands were detected

with the MicroChemi system (DNR Bio-Imaging Systems Ltd.) and quantified using ImageJ software.

Flow cytometry and cell sorting. Multicolor flow cytometry and cell sorting were performed with an LSR Fortessa and BD FACSAria III cell sorter using DIVA software (BD Biosciences) as previously described (16, 70). Cells ($1–5 \times 10^5$) from AEC cell cultures or derived from lavaged, perfused, and homogenized murine lungs were freshly stained with fluorochrome-labeled antibodies for 15 minutes at 4°C in BD FACS buffer (BD Biosciences). When nonlabeled primary monoclonal antibody was used, a fluorescent-labeled secondary antibody was incubated for 15 minutes at 4°C in FACS buffer. Cells were routinely stained with 7-AAD (BioLegend) for dead cell exclusion, and were also stained with antibodies to detect CD326 (clone G8.8, BioLegend), CD74 (clone ln-1, BD Biosciences), Podoplanin (clone 8.1., BioLegend), polyclonal IAV (clone ab20841, Abcam), NKAα1, CD45 (clone 30-F11, BioLegend), GR-1 (clone RB6-8C5, BioLegend), Ly6G (clone 1A8, BioLegend), SiglecF (clone E50-2440, BD Biosciences), CD11c (clone N418, BioLegend), CD11b (clone M1/70, BioLegend), secondary goat APC (clone A21447, Invitrogen), and secondary rat PE (clone A10545, Invitrogen) . Corresponding isotype antibodies were used as negative controls. For annexin V staining, cells were resuspended in annexin V staining buffer (10 mM HEPES, 140 mM NaCl, and 2.5 mM $CaCl_2$) and incubated with annexin V Alexa Fluor 647 (1:100, Invitrogen) for 15 minutes at 4°C. Data are presented as median fluorescent intensity (MFI) and were normalized to control groups set to 1 for in vitro experiments. $NKA\alpha1^+$ AEC from in vivo–infected mice are given as a percentage of the epithelial ($EpCAM^+$) cell population.

ELISA. Cell culture supernatants were analyzed using commercially available ELISA kits for mouse TRAIL (R&D Systems, detection limit 1.8 pg/ml) and mouse IFNα (PBL Interferon Source, detection limit 12.5 pg/ml), according to the manufacturer's instructions.

Quantitative PCR. RNA was isolated using RNeasy Kit (QIAGEN) and cDNA synthesized as described previously (66). Quantitative PCR (qPCR) was performed with SYBR green I (Invitrogen) in the AB StepOnePlus Detection System (Applied Bioscience). β-Actin expression served as normalization control. Data are presented as ddCt ($dCt_{reference} - dCt_{target}$) or fold-change ($2^{\Delta\Delta Ct}$). The following primers were used: β-actin (forward primer, 5′-ACCCTAAGGCCAACCGTGA-3′; reverse primer, 5′-CAGAGGCATACAGGGACAGCA-3′); TRAIL (forward primer, 5′-GAAGACCTCAGAAAGTGGC-3′; reverse primer, 5′-GACCAGCTCTCCATTCTTA-3′).

Pulmonary transfer of BMM. BMM of WT or *Trail*$^{-/-}$ mice recruited to the alveolar compartment after IAV challenge with 500 pfu PR8 were obtained by bronchoalveolar lavage on d7 pi after challenge with 500 pfu PR8. BMM were identified by the signature $CD45^+GR\text{-}1^+Ly6G^-CD11b^{hi}CD11c^{lo}SiglecF^{lo}$ and flow sorted (Supplemental Figure 5). The purity of sorted BMM (≥95%) was ensured by flow cytometric analysis, as well as by pappenheim stained cytospins. Sorted BMM were resuspended in sterile PBS, and 30,000 cells in 50 μl were transferred intratracheally to PR8-infected *Ccr2*$^{-/-}$ mice on d3 pi; the mice were analyzed for Na,K-ATPase–mediated fluid clearance on d7 pi.

Statistics. All data are given as mean ±SEM. Statistical significance was analyzed by unpaired 2-tailed Student's *t* test or by 1-way ANOVA and post-hoc Tukey (GraphPad Prism 5). A *P* value less than 0.05 was considered significant. $^*P < 0.05$; $^{**}P < 0.01$; $^{***}P < 0.005$.

Study approval. Animal experiments were approved by the regional authorities of the State of Hesse (Regierungspräsidium Giessen) and by the Institutional Animal Care and Use Committee at Northwestern University. Human lung tissue was obtained from patients who underwent lobectomy after informed written consent. Use of human lung tissue and BALF samples was approved by the University of Giessen Ethics Committee.

Author contributions

CP, CS, IV, TW, SP, REM, JL, WS, and SH were involved in study design and concept. Data were acquired by CP, BS, LMN, EL, JB, LF, and SG. GMM and GRSB were involved in the AFC measurements. Data analysis, interpretation, and statistics was conducted by CP, EL, KM, JL, JIS, IV, and SH. CP, CS, JL, JIS, and SH drafted the manuscript.

Acknowledgments

This study was supported by the German Research Foundation (SFB-TR84 B2, IRTG1062, SFB1021 C05, EXC147 to S. Herold, J. Lohmeyer, W. Seeger, S. Pleschka, and T. Wolff) by the German Federal Ministry of Research and Education ("FluResearchNet" 01 KI 1006M to S. Herold and J. Lohmeyer), and by DZL (to S. Herold, J. Lohmeyer, W. Seeger, I. Vadász, K. Mayer, L. Fink, and R.E. Morty), by ES015024 and ES025644 (to G.M. Mutlu), and by HL-48129 and 71643 (to G.R.S. Budninger and J.I. Sznajder). The authors wish to thank U. Kalinke, and T. Mak for providing transgenic mice.

Address correspondence to: Susanne Herold, Universities Giessen & Marburg Lung Center, Department of Internal Medicine II, Klinikstr. 33, D-35392 Giessen, Germany. Phone: 49.641.985.42552; E-mail: Susanne.Herold@innere.med.uni-giessen.de.

1. Jain S, et al. Hospitalized patients with 2009 H1N1 influenza in the United States, April–June 2009. *N Engl J Med*. 2009;361(20):1935–1944.
2. Short KR, Kroeze EJ, Fouchier RA, Kuiken T. Pathogenesis of influenza-induced acute respiratory distress syndrome. *Lancet Infect Dis*. 2014;14(1):57–69.
3. Kuiken T, Taubenberger JK. Pathology of human influenza revisited. *Vaccine*. 2008;26(suppl 4):D59–D66.
4. Herold S, et al. Lung epithelial apoptosis in influenza virus pneumonia: the role of macrophage-expressed TNF-related apoptosis-inducing ligand. *J Exp Med*. 2008;205(13):3065–3077.
5. Matthay MA, Ware LB, Zimmerman GA. The acute respiratory distress syndrome. *J Clin Invest*. 2012;122(8):2731–2740.
6. Sznajder JI. Alveolar edema must be cleared for the acute respiratory distress syndrome patient to survive. *Am J Respir Crit Care Med*. 2001;163(6):1293–1294.
7. Matthay MA. Alveolar fluid clearance in patients with ARDS: does it make a difference? *Chest*. 2002;122(6 suppl):340S–343S.
8. Folkesson HG, Matthay MA. Alveolar epithelial ion and fluid transport: recent progress. *Am J Respir Cell Mol Biol*. 2006;35(1):10–19.
9. Borok Z, Verkman AS. Lung edema clearance: 20 years of progress: invited review: role of aquaporin water channels in fluid transport in lung and airways. *J Appl Physiol*. 2002;93(6):2199–2206.
10. Machado-Aranda D, et al. Gene transfer of the Na^+,K^+-ATPase β1 subunit using electroporation increases lung liquid clearance. *Am J Respir Crit Care Med*. 2005;171(3):204–211.
11. Adir Y, et al. Overexpression of the Na-K-ATPase α2-subunit improves lung liquid clearance during ventilation-induced lung injury. *Am J Physiol Lung*

Cell Mol Physiol. 2008;294(6):L1233–L1237.
12. Lecuona E, Trejo HE, Sznajder JI. Regulation of Na,K-ATPase during acute lung injury. *J Bioenerg Biomembr*. 2007;39(5–6):391–395.
13. Mutlu GM, Sznajder JI. Mechanisms of pulmonary edema clearance. *Am J Physiol Lung Cell Mol Physiol*. 2005;289(5):L685–L695.
14. Bertorello AM, et al. Analysis of Na^+,K^+-ATPase motion and incorporation into the plasma membrane in response to G protein-coupled receptor signals in living cells. *Mol Biol*. 2003;14(3):1149–1157.
15. Saldías FJ, et al. β-Adrenergic stimulation restores rat lung ability to clear edema in ventilator-associated lung injury. *Am J Respir Crit Care Med*. 2000;162(1):282–287.
16. Högner K, et al. Macrophage-expressed IFN-β contributes to apoptotic alveolar epithelial cell injury in severe influenza virus pneumonia. *PLoS Pathog*. 2013;9(2):e1003188.
17. Wolk KE, et al. Influenza A virus inhibits alveolar fluid clearance in BALB/c mice. *Am J Respir Crit Care Med*. 2008;178(9):969–976.
18. Baskin CR, et al. Early and sustained innate immune response defines pathology and death in nonhuman primates infected by highly pathogenic influenza virus. *Proc Natl Acad Sci U S A*. 2009;106(9):3455–3460.
19. De Jong MD, et al. Fatal outcome of human influenza A (H5N1) is associated with high viral load and hypercytokinemia. *Nat Med*. 2006;12(10):1203–1207.
20. Bertorello AM, Ridge KM, Chibalin AV. Katz AI, Sznajder JI. Isoproterenol increases Na^+-K^+-ATPase activity by membrane insertion of α-subunits in lung alveolar cells. *Am J Physiol*. 1999;276(1):L20–L27.
21. Lecuona E, Sun H, Vohwinkel C, Ciechanover A, Sznajder JI. Ubiquitination participates in the lysosomal degradation of Na,K-ATPase in steady-state conditions. *Am J Respir Cell Mol Biol*. 2009;41(6):671–679.
22. Factor P, et al. Augmentation of lung liquid clearance via adenovirus-mediated transfer of a Na,K-ATPase β1 subunit gene. *J Clin Invest*. 1998;102(7):1421–1430.
23. Factor P, et al. Overexpression of the Na^+,K^+-ATPase α1 subunit increases Na^+,K^+-ATPase function in A549 cells. *Am J Respir Cell Mol Biol*. 1998;18(6):741–749.
24. Mutlu GM, et al. Upregulation of alveolar epithelial active Na^+ transport is dependent on β2-adrenergic receptor signaling. *Circ Res*. 2004;94(8):1091–1100.
25. Barut S, et al. The neuroprotective effects of z-DEVD.fmk, a caspase-3 inhibitor, on traumatic spinal cord injury in rats. *Surg Neurol*. 2005;64(3):213–220.
26. Knoblach SM, et al. Caspase inhibitor z-DEVD-fmk attenuates calpain and necrotic cell death in vitro and after traumatic brain injury. *J Cereb Blood Flow Metab*. 2004;24(10):1119–1132.
27. Gusarova G, a et al. Hypoxia leads to Na,K-ATPase downregulation via Ca(2+) release-activated Ca(2+) channels and AMPK activation. *Mol Cell Biol*. 2011;31(17):3546–3556.
28. Vadász I, et al. AMP-activated protein kinase regulates CO2-induced alveolar epithelial dysfunction in rats and human cells by promoting Na,K-ATPase endocytosis. *J Clin Invest*. 2008;118(2):752–762.
29. Park SH, et al. Phosphorylation-activity relationships of AMPK and acetyl-CoA carboxylase in muscle. *J Appl Physiol*. 2002;92(6):2475–2482.
30. Kaushik VK, et al. Regulation of fatty acid oxidation and glucose metabolism in rat soleus muscle: effects of AICAR. *Am J Physiol Endocrinol Metab*. 2001;281(2):E335–E340.
31. Sullivan JE, et al. Inhibition of lipolysis and lipogenesis in isolated rat adipocytes with AICAR, a cell-permeable activator of AMP-activated protein kinase. *FEBS Lett*. 1994;353(1):33–36.
32. Zhou G, et al. Role of AMP-activated protein kinase in mechanism of metformin action. *J Clin Invest*. 2001;108(8):1167–1174.
33. Witczak CA, Sharoff CG, Goodyear LJ. AMP-activated protein kinase in skeletal muscle: from structure and localization to its role as a master regulator of cellular metabolism. *Cell Mol Life Sci*. 2008;65(23):3737–3755.
34. Ninomiya-Tsuji J, et al. A resorcylic acid lactone, 5Z-7-oxozeaenol, prevents inflammation by inhibiting the catalytic activity of TAK1 MAPK kinase kinase. *J Biol Chem*. 2003;278(20):18485–18490.
35. Herold S, et al. Alveolar epithelial cells direct monocyte transepithelial migration upon influenza virus infection: impact of chemokines and adhesion molecules. *J Immunol*. 2006;177(3):1817.
36. Lazrak A, et al. Influenza virus M2 protein inhibits epithelial sodium channels by increasing reactive oxygen species. *FASEB J*. 2009;23(11):3829–3842.
37. Londino JD, et al. Influenza matrix protein 2 alters CFTR expression and function through its ion channel activity. *Am J Physiol Lung Cell Mol Physiol*. 2013;304(9):L582–L592.
38. Jewell NA, et al. Differential type I interferon induction by respiratory syncytial virus and influenza a virus in vivo. *J Virol*. 2007;81(18):9790–9800.
39. Hayden FG, et al. Local and systemic cytokine responses during experimental human influenza A virus infection. Relation to symptom formation and host defense. *J Clin Invest*. 1998;101(3):643–649.
40. Arimori Y, et al. Type I interferon limits influenza virus-induced acute lung injury by regulation of excessive inflammation in mice. *Antiviral Res*. 2013;99(3):230–237.
41. Steel J, et al. Transmission of pandemic H1N1 influenza virus and impact of prior exposure to seasonal strains or interferon treatment. *J Virol*. 2010;84(1):21–26.
42. Kugel D, et al. Intranasal administration of alpha interferon reduces seasonal influenza A virus morbidity in ferrets. *J Virol*. 2009;83(8):3843–3851.
43. Tumpey TM, et al. Pathogenicity of influenza viruses with genes from the 1918 pandemic virus: functional roles of alveolar macrophages and neutrophils in limiting virus replication and mortality in mice. *J Virol*. 2005;79(23):14933–14944.
44. Lin KL, Suzuki Y, Nakano H, Ramsburg E, Gunn MD. CCR2+ monocyte-derived dendritic cells and exudate macrophages produce influenza-induced pulmonary immune pathology and mortality. *J Immunol*. 2008;180(4):2562–2572.
45. Chan M et al. Proinflammatory cytokine responses induced by influenza A (H5N1) viruses in primary human alveolar and bronchial epithelial cells. *Respir Res*. 2005;6(135):1–13.
46. Herold S, Becker C, Ridge KM, Budinger GRS. Influenza virus-induced lung injury: pathogenesis and implications for treatment. *Eur Respir J*. 2015;45(5):1463–1478.
47. Kim HM, et al. Alveolar macrophages are indispensable for controlling influenza viruses in lungs of pigs. *J Virol*. 2008;82(9):4265–4274.
48. Walsh KB, et al. Suppression of cytokine storm with a sphingosine analog provides protection against pathogenic influenza virus. *Proc Natl Acad Sci U S A*. 2011;108(29):12018–12023.
49. Van Reeth K. Cytokines in the pathogenesis of influenza. *Vet Microbiol*. 2000;74(1–2):109–116.
50. Szretter KJ, et al. Role of host cytokine responses in the pathogenesis of avian H5N1 influenza viruses in mice. *J Virol*. 2007;81(6):2736–2744.
51. To KK, et al. Delayed clearance of viral load and marked cytokine activation in severe cases of pandemic H1N1 2009 influenza virus infection. *Clin Infect Dis*. 2010;50(6):850–859.
52. Davidson S, Crotta S, McCabe TM, Wack A. Pathogenic potential of interferon αβ in acute influenza infection. *Nat Commun*. 2014;5:3864.
53. Baritaki S, et al. Regulation of tumor cell sensitivity to TRAIL-induced apoptosis by the metastatic suppressor Raf kinase inhibitor protein via Yin Yang 1 inhibition and death receptor 5 up-regulation. *J Immunol*. 2007;179(8):5441–5453.
54. Song K, Benhaga N, Anderson RL, Khosravi-Far R. Transduction of tumor necrosis factor-related apoptosis-inducing ligand into hematopoietic cells leads to inhibition of syngeneic tumor growth in vivo. *Cancer Res*. 2006;66(12):6304–6311.
55. Liu C, Liang B, Wang Q, Wu J, Zou MH. Activation of AMP-activated protein kinase alpha1 alleviates endothelial cell apoptosis by increasing the expression of anti-apoptotic proteins Bcl-2 and survivin. *J Biol Chem*. 2010;285(20):15346–15355.
56. Hardie DG, Scott JW, Pan DA, Hudson ER. Management of cellular energy by the AMP-activated protein kinase system. *FEBS Lett*. 2003;546(1):113–120.
57. Herrero-Martín G, et al. TAK1 activates AMPK-dependent cytoprotective autophagy in TRAIL-treated epithelial cells. *EMBO J*. 2009;28(6):677–685.
58. Moseley CE, Webster RG, Aldridge JR. Peroxisome proliferator-activated receptor and AMP-activated protein kinase agonists protect against lethal influenza virus challenge in mice. *Influenza Other Respi*. 2010;4(5):307–311.
59. Hoffmann HH, Palese P, Shaw ML. Modulation of influenza virus replication by alteration of sodium ion transport and protein kinase C activity. *Antiviral Res*. 2008;80(2):124–134.
60. Wang L, et al. "Tuning" of type I interferon-induced Jak-STAT1 signaling by calcium-dependent kinases in macrophages. *Nat Immunol*. 2008;9(2):186–193.
61. Ellis GT, Davidson S, Crotta S, Branzk N, Papayannopoulos V, Wack A. TRAIL+ monocytes

and monocyte-related cells cause lung damage and thereby increase susceptibility to influenza-Streptococcus pneumoniae coinfection. *EMBO Rep*. 2015;16(9):1203–1218.
62. Cretney E, et al. Increased susceptibility to tumor initiation and metastasis in TNF-related apoptosis-inducing ligand-deficient mice. *J Immunol*. 2002;168(3):1356–1361.
63. Müller U, et al. Functional role of type I and type II interferons in antiviral defense. *Science*. 1994;264(5167):1918–21.
64. Finnberg N, et al. DR5 knockout mice are compromised in radiation-induced apoptosis. *Mol Cell Biol*. 2005;25(5):2000–2013.
65. Kuziel WA, et al. Severe reduction in leukocyte adhesion and monocyte extravasation in mice deficient in CC chemokine receptor 2. *Proc Natl Acad Sci U S A*. 1997;94(22):12053–12058.
66. Cakarova L, et al. Macrophage tumor necrosis factor-alpha induces epithelial expression of granulocyte-macrophage colony-stimulating factor: impact on alveolar epithelial repair. *Am J Respir Crit Care Med*. 2009;180(6):521–532.
67. Barwe SP, et al. Novel role for Na,K-ATPase in phosphatidylinositol 3-kinase signaling and suppression of cell motility. *Mol Biol*. 2005;16(3):1082–1094.
68. Hardiman KM, Lindsey JR, Matalon S. Lack of amiloride-sensitive transport across alveolar and respiratory epithelium of iNOS(–/–) mice in vivo. *Am J Physiol Lung Cell Mol Physiol*. 2001;281(3):L722–731.
69. Dada LA, et al. Hypoxia-induced endocytosis of Na,K-ATPase in alveolar epithelial cells is mediated by mitochondrial reactive oxygen species and PKC-ζ. *J Clin Invest*. 2003;111(7):1057–1064.
70. Unkel B, et al. Alveolar epithelial cells orchestrate DC function in murine viral pneumonia. *J Clin Invest*. 2012;122(10):3652–3664.